Crack initiation in VHCF regime on forged titanium alloy under tensile and torsion loading modes

Alexander Nikitin, Thierry Palin-Luc, Andrey Shanyavskiy

Crack initiation in VHCF regime on forged titanium alloy under tensile and torsion loading modes

A. Nikitin [a,b], T. Palin-Luc [c], A. Shanyavskiy [b,d,*]

[a] LEME, University Paris Ouest Nanterre La Defense, 50, rue de Serves, Ville-d'Avray 92410, France
[b] MAI – National Research University, 4, Volokolamskoe Hwy, A-80, GSP-3, Moscow 125993, Russia
[c] Arts et Metiers Paris Tech, I2M, CNRS, Universite de Bordeaux, Esplanade des Arts et Metiers, Talence 33405, France
[d] Aviaregister, Air. Sheremetevo-1, PO Box 54, Moscow reg., Chimkovskiy state, 141426, Russia

A B S T R A C T

This paper is focused on the VHCF behavior of aeronautical titanium alloy under tensile and torsion fatigue loadings. Tensile tests were carried out with two different stress ratios: $R = -1$ and $R = 0.1$. Both surface and subsurface crack initiations were observed. In the case of subsurface crack initiation several fatigue life controlling mechanisms of crack initiation were found under fully-reversed loading conditions: initiation from (1) strong defects; (2) 'macro-zone' borders; (3) quasi-smooth facets and (4) smooth facets. Tests with stress ratio $R = 0.1$, have shown that initiation from the borders of 'macro-zones' becomes the dominant crack initiation mechanism in presence of positive mean stress. Like for the tensile results, surface and subsurface crack initiations were observed under ultrasonic torsion in spite of the maximum shear stress location on the specimen surface. But the real reason for the subsurface crack initiation under torsion was not found.

Keywords:
Very-high cycle fatigue
Titanium alloy
Crack initiation
Ultrasonic torsion

1. Introduction

The problem of fatigue in aeronautical application has a long history [1,2] and for a long time it was assumed (considered) as low (LCF) and high cycle fatigue (HCF) problems. These two domains were deeply studied for different aeronautical materials, such as aluminum, titanium and nickel based alloys [3]. However, in spite of the developed knowledge about the fatigue behavior of aeronautical materials in the LCF and HCF regimes, some 'unexpected' in-service failures were reported [4–6] for compressor and turbine. One of the most critical elements of the aircraft in terms of 'unexpected failure' is the turbojet engine. The analysis of typical loading spectrum for blades of turbojet engine has shown that the number of loading cycles for such application can reach 10^{10} cycles during in service [7]. The regime of fatigue with ultra long fatigue life is known as very high cycle fatigue (VHCF) or Gigacycle fatigue. Convenient experimental methods are proposed to estimate the fatigue strength at much lower fatigue life (about 10^7, maximum 10^8 cycles) that is 2–3 orders of magnitude shorter compared to the real life. Consequently, conclusion of Nicholas [4] about a premature in-service fatigue failure of titanium compressor of military aircraft was the following: 'unexpected fatigue failure was due to high frequency loading that lead to accumulation about 10^9 loading cycles during in-service'. Moreover, the fatigue behavior of material in VHCF regime is very sensitive to microstructural features of materials that lead to different types of SN-curves [8]. Therefore, nowadays it is impossible to determine the parameters of the SN-curve of a material in VHCF regime without experiment.

Usually the critical stress–strain state of fatigue on real elements is estimated by using multiaxial criteria. However, there are no ultrasonic testing methods for multi-axial loading. The only solution for developing multiaxial criteria in VHCF regime is using several testing systems for different loading conditions. Bathias has developed numerous of ultrasonic testing machines such as tension–compression, tension–tension, three points bending [9], torsion [10] and some other systems [7,11]. It has been shown that the crack initiation mechanism under different loading conditions can be different.

The purpose of this work is to investigate the crack initiation mechanisms in aeronautical VT3-1 titanium alloy under different loading conditions. Tensile tests under different load ratios were performed together with ultrasonic torsion. Fracture surfaces of all the tested specimens were investigated by SEM in order to identify the crack initiation mechanism.

* Corresponding author at: Aviaregister, Air. Sheremetevo-1, PO Box 54, Moscow reg., Chimkovskiy state, 141426, Russia.
E-mail addresses: nikitin_alex@bk.ru (A. Nikitin), thierry.palin-luc@ensam.eu (T. Palin-Luc), shananta@mailfrom.ru (A. Shanyavskiy).

2. Material and experimental procedure

2.1. Material

The studied material in the present work is the forged VT3-1 titanium alloy that is commonly used in the aeronautic industry for compressor disks and blades production. All the specimens were machined from a real compressor disk of a D30 turbojet engine used for Tu-154 aircraft, Fig. 1a.

The disk has flown about 16,000 h. The in-service flown disk was submitted to non destructive controls (ultrasonic NDT and alternating current field measurement) in order to estimate possible accumulated in-service fatigue damages. The results of this after service controls did not reveal degradation of the material due to fatigue (no cracks or material defects). The chemical composition of forged titanium alloy respects to the State standards [12], (Table 1).

The microstructure of this forged VT3-1 titanium alloy is shown in Fig. 2a. One can see by elongated alpha-platelets with typical length of 10–15 μm and width of 2–3 μm, Fig. 2b. Macroscopically the microstructure of this titanium alloy is strongly inhomogeneous with clear alpha-platelets agglomerations of different sizes and shapes, Fig. 2c. Besides local agglomerations the microstructure is also represented by large continuous areas that are filled with thin, similarly orientated alpha-platelets, Fig. 2d. Such areas were already observed in a forged titanium alloy and reported in the literature as 'macro-zones' [13].

The micro-hardness of this titanium alloy is also inhomogeneous that is stated based on measurements along the specimen's cross-section diameter. The average value of micro-hardness is 364 HV500 with a maximum deviation of 44 HV500. The value of micro-hardness is related to geometry of alpha-platelets at the location of measurement. Where there is an agglomeration of rough alpha-platelets the micro-hardness value is higher compared to the areas with finer platelets (398 HV for rough and 238 HV for fine alpha-platelets).

The mechanical properties were studied by using small tensile specimens machined from the disk's web, Fig. 1. Blanks for tensile specimen were taken in circumferential direction. Flat tensile specimens had a thickness of 1 mm, a total length of 75 mm, a length of the working section of 25 mm and a working section width of 5 mm. Monotonic tensile tests were carried out with a displacement rate of 0.075 mm/min. Additionally, the dynamic modulus was determined at 20 kHz. All the mechanical properties are given in Table 2.

2.2. Experimental procedures

Two types of fatigue tests in VHCF regime (tensile and torsion) were carried out by using ultrasonic fatigue testing systems. Tensile fatigue tests were performed on a LASUR piezoelectric machine [7] under fully reversed ($R = -1$) and asymmetric ($R = 0.1$) loadings at 20 kHz up to the specimen failure or run-out limit of 5×10^9 cycles for the tensile tests and 10^9 cycles for the torsion one. The torsion fatigue tests were performed on a self-designed piezoelectric torsion system [14] under fully-reversed ($R = -1$) loading. All the tests were carried out in laboratory air at room temperature (compressed air cooling). The temperature of the specimen surface was measured by infrared camera measurements for some of the tested specimens. To do that, some tensile and torsion specimens were painted in matt black for the tests with surface temperature measurement at different stress levels (from 100 to 400 MPa for tensile tests and 240 MPa for torsion). All the tests were performed with air cooling (like under all the fatigue tests) and a base for one

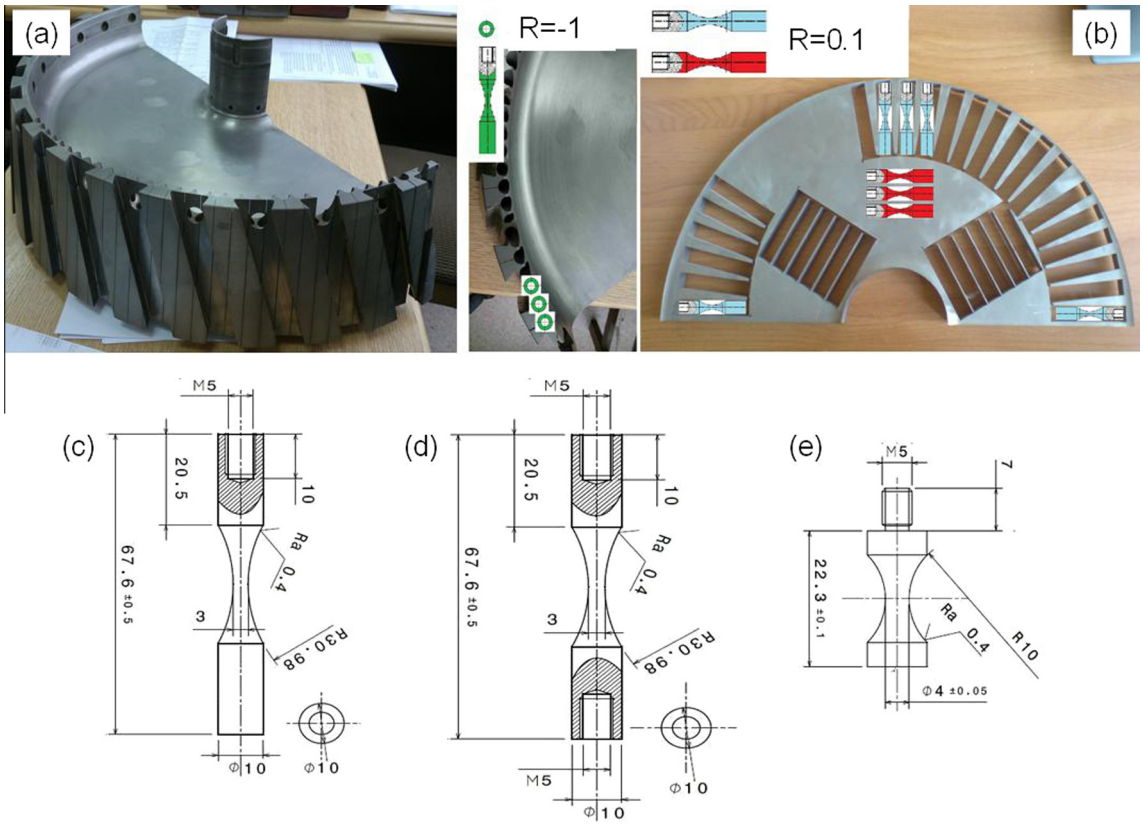

Fig. 1. Compressor disk of D30 turbojet engine (a), location of specimens in the disk (b), (c) and (d) geometries of tensile specimens, (e) geometry of torsion specimen, (all the dimensions are in mm).

Table 1
Chemical composition of forged VT3-1 titanium alloy (wt%).

Fe	C	Si	Cr	Mo	N	Al	Zr	O	H
0.2–0.7	<0.1	0.15–0.4	0.8–2	2–3	<0.05	5.5–7	<0.5	<0.15	<0.015

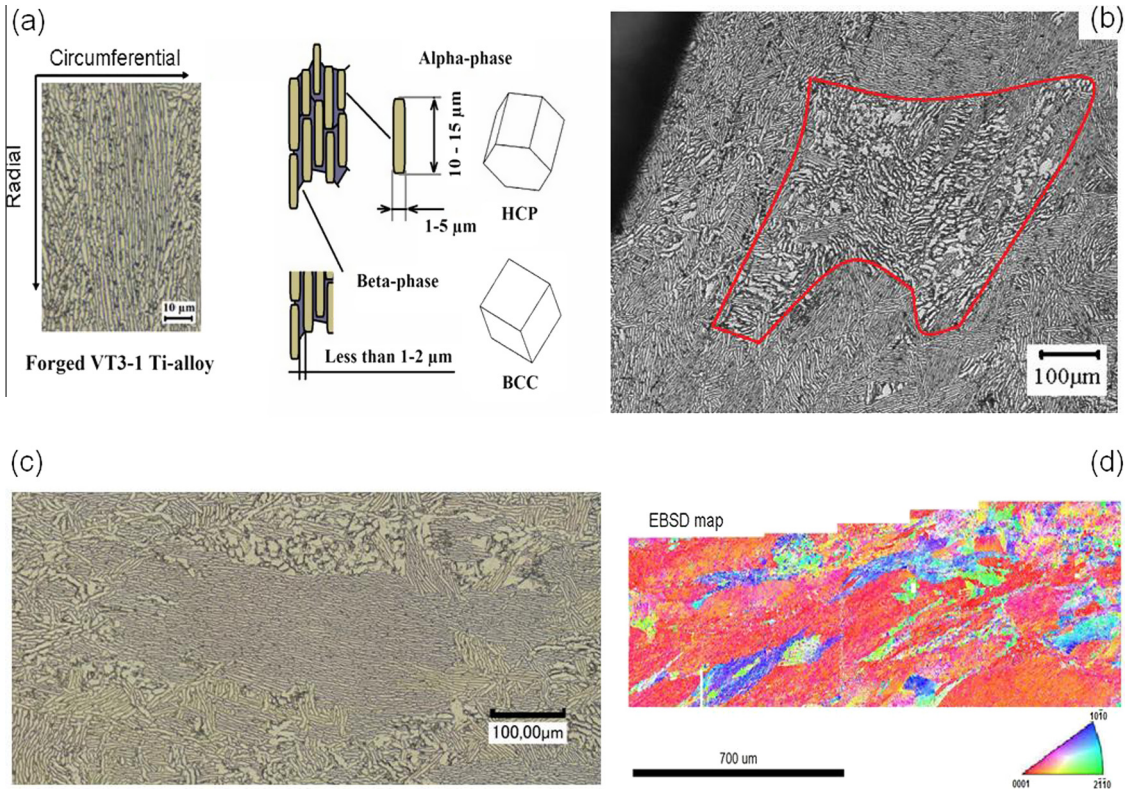

Fig. 2. Microstructure of forged VT3-1 titanium alloy (a) with typical alpha-platelets (b) that can form agglomerations of different shapes (c) and macro-zones clearly visible by EBSD (d).

Table 2
Mechanical properties of forged VT3-1 titanium alloy.

Young's modulus, (GPa)	UTS (MPa)	Yieldstress (MPa)	Elongation at rupture (%)	Volumetric mass (kg m^{-3})	Dynamic modulus (GPa)
114	989	960	6	4500	116

test was 5×10^6 cycles. It was pointed out that at each load level the surface temperature gets stable (horizontal line on graph temperature versus time) after a few seconds of the test. The results of these tests have shown that the maximum increase of temperature due to self heating was less than 10 °C [14].

Specimens for ultrasonic fatigue tests were machined from different areas of the compressor disk, Fig. 1b. Tensile fatigue specimens, Fig. 1c and d were machined from both the rim and the web parts of the disk while torsion specimens, Fig. 1e, were cut from the rim part only. Several sets of tensile fatigue specimens were prepared: (1) specimens for fully-reversed ($R = -1$) tests were machined from the rim part in axial direction, Fig. 1b and from web part in radial direction; (2) specimens for asymmetric ($R = 0.1$) tests were machined from web part in radial and circumferential directions, Fig. 1b. The surface of all the specimens was mechanically polished with emery paper up to grade 1000. Machining and mechanical polishing may introduce ~~a~~ residual stresses that could affect the crack initiation mechanism. These residual stresses could lead to near surface crack initiation. Such influence of residual stresses was already discussed for the case of ultrasonic torsion tests on steels. It was found that subsurface torsion crack can initiate from the subsurface in the presence of high residual stresses [15]. In the present study the residual stresses were not measured due to limitations of X-ray diffraction instrument because of the complex microstructure of this alloy. The uncertainty of the measurements was higher than the measured values.

3. Results and discussions

3.1. Tensile fully-reversed ($R = -1$) tests

The results of the tests are presented in Fig. 3. As usual with increasing stress amplitude the fatigue life decreases but we can observe very large scatter. In HCF regime fatigue failures were mainly observed under stress amplitudes of 415–430 MPa that is about 43% of ultimate tensile strength. However, there is one stand out result that was obtained under lower stress amplitude after a short fatigue life (in HCF regime). The fracture surface analysis by SEM for this specimen has shown subsurface crack initiation with quite damaged origination site. It seems that such initiation is related to some sort of microstructural defect that was not yet found on observed micro-sections. The results of the fatigue tests show a large scatter of fatigue life that reach three orders of magnitude under certain stress amplitudes. In spite of so large scatter a

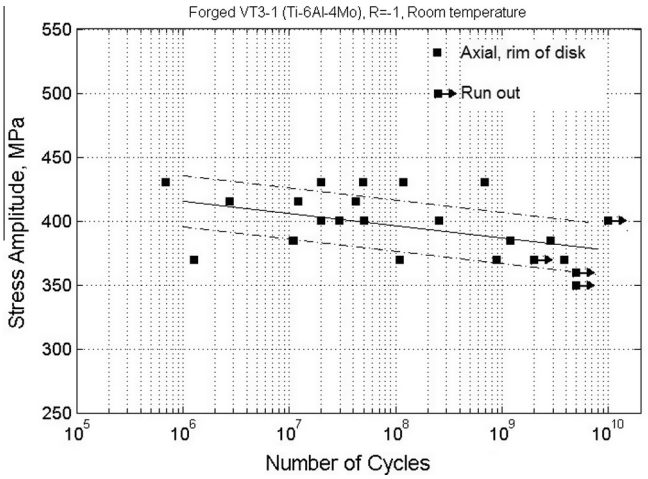

Fig. 3. The SN-curve for forged VT3-1 titanium alloy under fully-reversed ($R = -1$) tensile fatigue loading at 20 kHz.

trend line built by least square method is straight decreasing line with clear slope of the SN-curve. Thus, we can say that forged VT3-1 does not show a horizontal asymptote like many others structural materials [8] and there is no infinite fatigue life [16,17]. A similar result has been reported for Ti–6Al–4V titanium alloy by Janecek [18] in VHCF regime under fully-reversed loading ($R = -1$) at 20 kHz. It has been stated that the SN curves exhibit a continuous decrease of the stress amplitude with increasing number of cycles from 10^4 to 10^9 cycles.

In our experiments the analysis of the fracture surfaces has shown two principal crack initiation locations: surface and subsurface. This result is common for two-phase titanium alloy and was already reported for different alloy [18,19]. However, in order to understand the reason of so large scatter of the fatigue life (Fig. 3), the fracture surface of all the specimens was analyzed by using scanning electron microscope (SEM). From these fractographic analyses it was found that under high stress amplitudes and short fatigue life crack initiation site is observed at the specimen surface. Detailed analysis on crack initiation sites by SEM allows us to outline several 'fatigue life controlling' mechanisms. Specimens with shorter fatigue life and subsurface crack initiations have a strong defect of the microstructure at crack initiation site, Fig. 4a. Strong defects of microstructure produce a quasi-brittle pattern with clear traces of cracked alpha-platelets. The geometry of these quasi-brittle zones and traces of alpha-platelet allow us to associate these defects with an agglomeration of rough alpha-platelets, Fig. 2c.

With increasing the fatigue life the quota of specimens with crack initiation from strong defects is decreasing. In this case another crack initiation mechanism starts to dominate over the previous one. In longer fatigue life, fatigue crack is typically initiated from the border of 'macro-zones' that are large areas formed by similarly orientated alpha-platelets [13], Fig. 4b. Within such zone all the alpha-platelets have almost the same crystallographic orientation that allows easier dislocation moving on long distance. The border of two 'macro-zones' is an important barrier for dislocation moving that makes the 'macro-zone' border a stock of a large number of dislocations. Micro-plasticity accumulated at 'macro-zones' borders lead to crack initiation.

The specimens failed after longest fatigue lives are typically showing two similar crack initiation sites: quasi-smooth and smooth facets, Fig. 4c and d respectively. These facets are formed due to failure of alpha-platelets or alpha-grains [20,21]. Fig. 4c and d illustrate a 3D model of individual alpha-platelet. In the case of quasi-smooth facet the alpha-platelet is broken (quasi-brittle fracture) along its elongation direction, Fig. 4c; in the case of the smooth facet, an individual alpha-platelet is broken by its cross section plane (Fig. 4). Moreover, the mechanisms of cracking is also different that can be clearly seen based on the analysis of the fracture surface morphologies around these facets. In the case of quasi-smooth facets around these facets a ductile fracture is observed with typical dimples and spherical particles while in the case of smooth facet the surrounded pattern shows a quasi brittle fracture. Both features are associated with a failure of individual alpha-platelet. The analysis of the chemical composition was performed by EDX module integrated into SEM. The chemical composition was studied within the crack initiation area: (1) from quasi-smooth facet where the following concentration of beta-stabilizing elements Mo and Cr were detected: molybdenum was 0.65wt%, chromium was not detected, Al was 8.72wt%; (2) from smooth facet: concentration of molybdenum was 0.59wt%, chromium was not detected and aluminum was 7.1wt%. It can be outlined that in the two cases the tendency is the same. There is a very low local concentration of Mo compared with the chemical composition of the VT3-1 alloy (Table 1) in which Mo content is between 2 and 3wt%.

Concluding the results of the fracture surfaces observations the following 'fatigue life controlling' mechanisms of subsurface crack initiation are: initiation from (1) strong defects; (2) border of macro-zones; (3) quasi-smooth facets and (4) smooth facets. According to these mechanisms a multi-modal interpretation of the SN-curve can be proposed, Fig. 5. According to this interpretation, we assume that a stress–strain incompatibility between 'matrix' and critical defect leads to premature failure. In the absence of critical defects on the plane of maximum stress the border of 'macro-zones' become a dominating crack initiation mechanism. However, the 'macro-zone' is characterized by its size and main crystallographic orientation. So, it means that not all the border has the same potential to block and accumulate dislocations. The crack is initiated from the border of two 'macro-zones' with unfavorable mutual orientation. In the case of absence of such adverse orientation, internal crack initiates from smaller features of the microstructure after longer fatigue life.

3.2. Tensile asymmetric (R = 0.1) tests

The results of the tests on forged VT3-1 titanium alloy with superimposed static stress ($R = 0.1$) are illustrated in Fig. 6(a). The character of fatigue strength decreasing (with the fatigue life) is similar to fully-reversed data and to the results of [19]. However, continuous decreasing of the fatigue strength versus the number of cycles is not always observed in the two-phase titanium alloy. For example in [22] it was reported about clear step of SN - curve for positive stress ratios. We also observed the same thing on the VT3-1 alloy. The results of tensile fatigue tests show a higher resistance of VT3-1 under $R = 0.1$ cyclic loads in terms of maximum stress. The fatigue strength of VT3-1 under fully-reversed loading is about 50 MPa lower compared to $R = 0.1$. However, representation of tensile fatigue results in Haigh diagram shows that the resistance of the forged VT3-1 titanium alloy against cyclic loading with imposed static stress is extremely low, Fig. 6(b). The results of fatigue tests under $R = 0.1$ are well below Gerber and Goodman predictions of fatigue strength. Such fatigue behavior of VT3-1 titanium alloy can be explained by using the idea of Oguma and Nakamura [22]. They have performed VHCF tests on Ti–6Al–4V titanium alloy under positive stress ratio $R = 0.1$. Titanium alloy was processed by two different treatments producing dual-phase microstructure with alpha-grains sizes of 4 and 10 μm respectively. Oguma and Nakamura have found that the alloy with the bigger alpha-grains has the lower fatigue strength. The difference in fatigue strength at 10^8 cycles between Ti-alloys with different

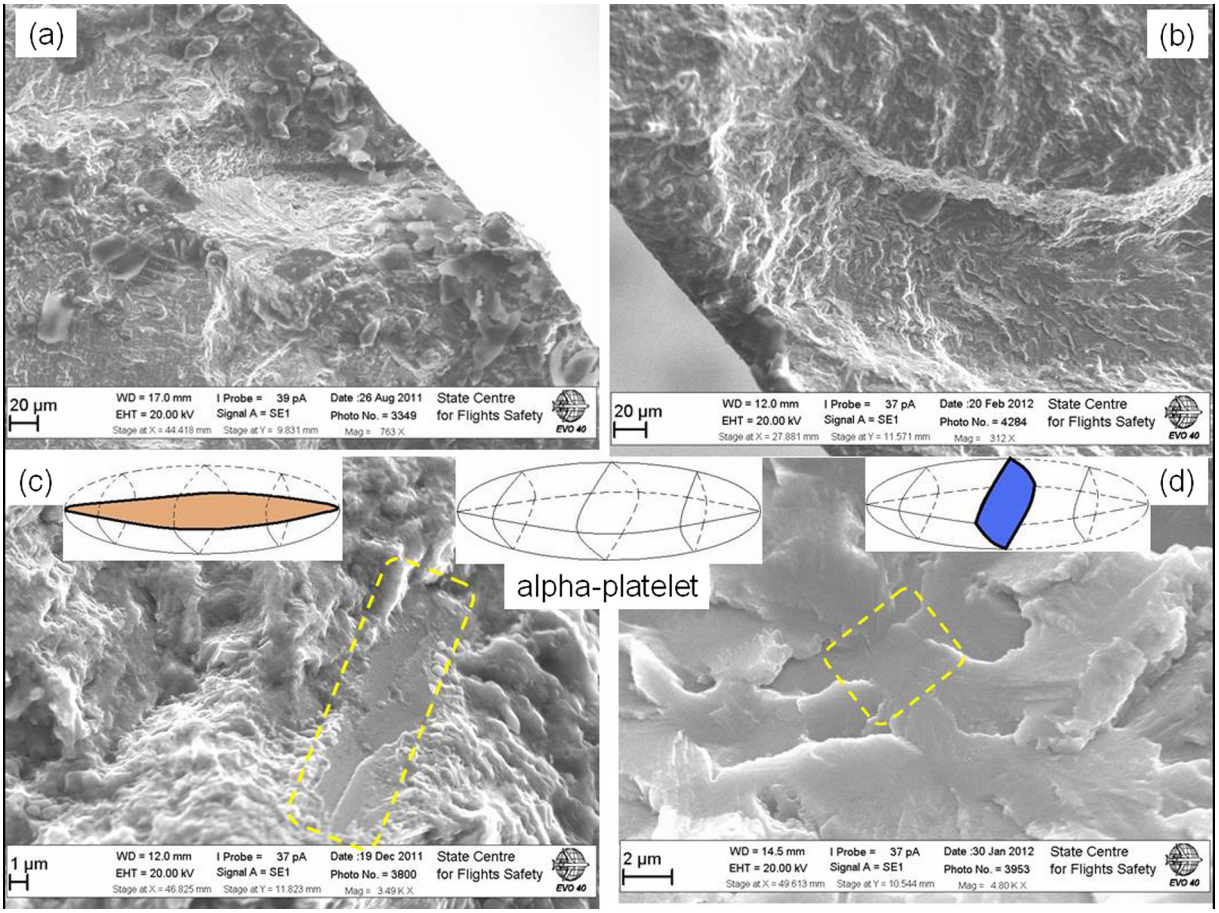

Fig. 4. Crack initiations in forged VT3-1 titanium alloy from (a) strong defect, (b) border of macro-zones, (c) quasi-smooth facet and (d) smooth facet.

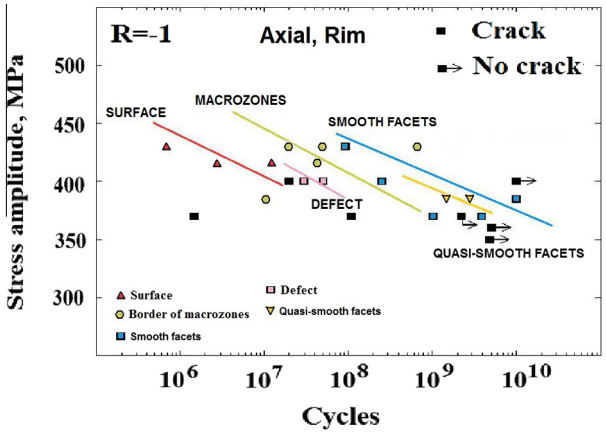

Fig. 5. Multi-modal SN-curve for forged VT3-1 under fully-reversed ($R = -1$) tensile loading at 20 kHz.

grain sizes was 180 MPa. They explain such fatigue behavior by larger 'effective slip length' in the material with the bigger grains. 'Macro-zones' of forged VT3-1 do also provide a large 'effective slip length' for dislocation motion that could lead to important drop of the fatigue strength. It means that the forged VT3-1 has a high sensitivity to static tensile stress in VHCF.

Under tensile ($R = 0.1$) the analysis of the fracture surfaces has shown that all the specimens failed because of subsurface crack initiation. All the specimens have crack initiation from the border of 'macro-zones', Fig. 7(a). It means that in the presence of static tensile stress initiation from the border of macro-zones becomes dominant. Further crack growth is also affected by 'macro-zones'.

The fracture pattern shows large zones (up to several hundred micrometers) of quasi-brittle fracture, Fig. 7(b), that is formed due to crack propagation by macro-zones. Probably quasi-brittle fracture is formed due to crack propagation by the border of 'macro-zones'. Some evidences of that can be observed on the fracture surface as small elements of neighboring structures in Fig. 7(c). Several "island-like" typical structures with different orientation of alpha-platelets within them were observed. The SEM analysis of these typical structures using back scattering mode has shown that the orientation of the alpha-platelets in these 'island-like' elements have a difference in the orientation of quasi-brittle fracture pattern, Fig. 7(d). Consequently, it seems that the crack propagates near or by the border of large macro-zones (agglomeration of alpha-platelets). Concluding results of SEM observation, it can be outlined that the extremely low resistance to cyclic loading of forged VT3-1 in VHCF regime in the presence of static tensile stress is due to large 'macro-zones'. These elements become critical under $R = 0.1$ tensile loading and leads to a significant drop of the VHCF strength.

3.3. Torsion fully-reversed ($R = -1$) tests

The results of ultrasonic torsion tests on forged VT3-1 alloy are presented on Fig. 8(a). These results show a fatigue strength decreasing with increasing number of loading cycles. Comparing the results of tensile and torsion ultrasonic tests it can be outlined

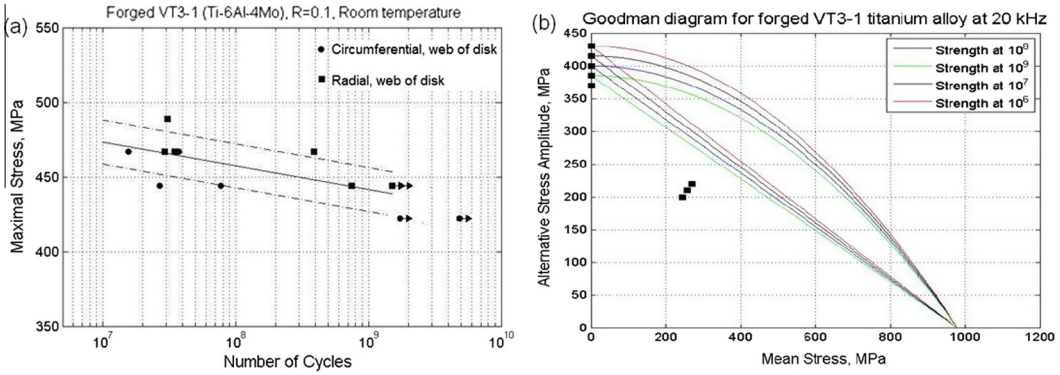

Fig. 6. (a) SN-curve for forged VT3-1 under asymmetric ($R = 0.1$) tensile loading and (b) Haigh diagram with Goodman and Gerber threshold.

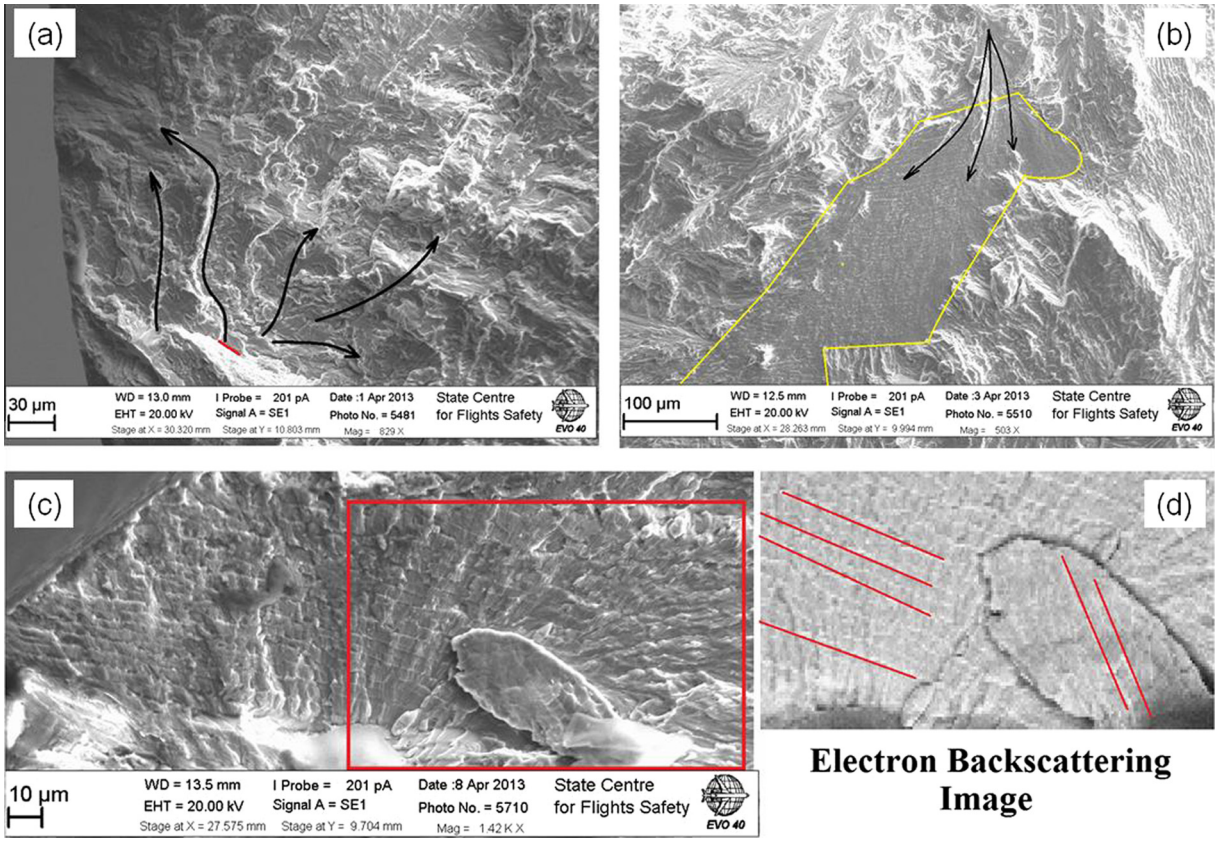

Fig. 7. Subsurface crack morphology in forged VT3-1 titanium alloy under $R = 0.1$ tensile loading (a) crack initiation from the border of macro-zone, (b) crack growth within macro-zones, (c) 'island-like' typical structure on the fracture pattern and (d) back scatter electrons image of 'island-like' structure.

that the slop of the torsion SN-curve is more pronounced. That can be clearly shown by using Von-Mises equivalent stress, Fig. 8(b).

The results of the fully reversed tensile and torsion tests presented in term of Von-Mises equivalent stress amplitude are close together and grouped around a fatigue strength of 400 MPa. The fatigue life range of specimens failed under torsion is being from (10^6 to 10^8 cycles). In the case of tensile loading subsurface crack initiation is mainly due to 'macro-zones'. Under torsion loading the specimens with the shortest fatigue life show surface crack initiation that is similar to high-cycle fatigue (HCF) regime. However, with decreasing stress amplitude the crack initiation site is shifted to the bulk of the material. It has been found that specimens failed beyond 10^8 cycles exhibit subsurface crack initiation.

Subsurface crack initiation is located at a distance of about 200 μm from the specimen surface, Fig. 9(a). The subsurface crack appears in the plane of maximum shear stress (perpendicular to the specimen's longitudinal axis). Fracture surface near the crack initiation area is significantly destroyed by friction due to contact between crack lips, Fig. 9(b). Therefore, it is impossible to identify a micro-structural feature that is responsible for crack initiation. Nevertheless, the fracture surface does not show clear crack growth by the border of macro-zones of large zones of quasi-brittle fracture that were observed under tensile loading. When crack becomes longer it bifurcates for propagating on the plane of maximum normal stress (inclined by 45 deg with respect to the specimen's axis). The analysis of the crack path at the specimen surface shows that the torsion crack growths on the plane of maximum normal stress up to the final length, Fig. 9(c). During this growth, crack may bifurcate to propagate on the maximum shear stress plane (perpendicular or parallel to the specimen axis) but

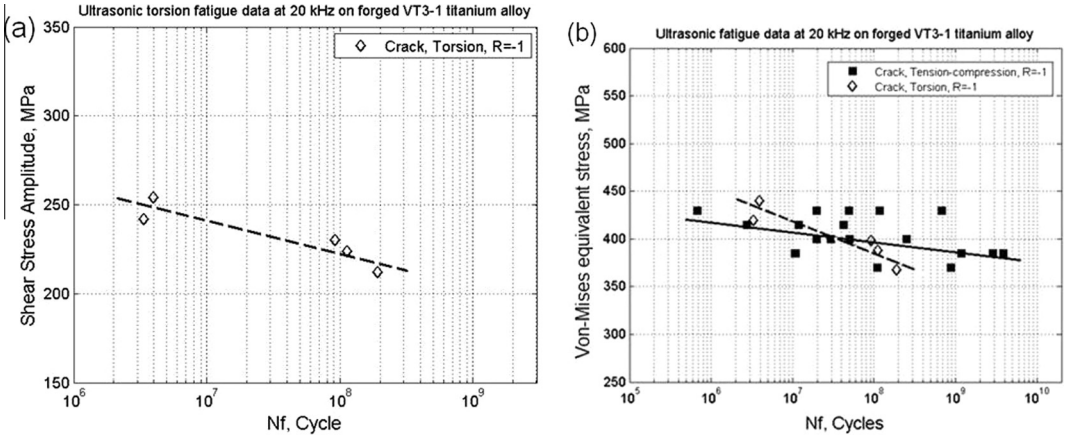

Fig. 8. SN-curve of the forged VT3-1 alloy under: (a) torsion ($R = -1$) in terms of shear stress amplitude and (b) tensile ($R = -1$) and torsion ($R = -1$) results in terms of Von-Mises equivalent stress amplitude.

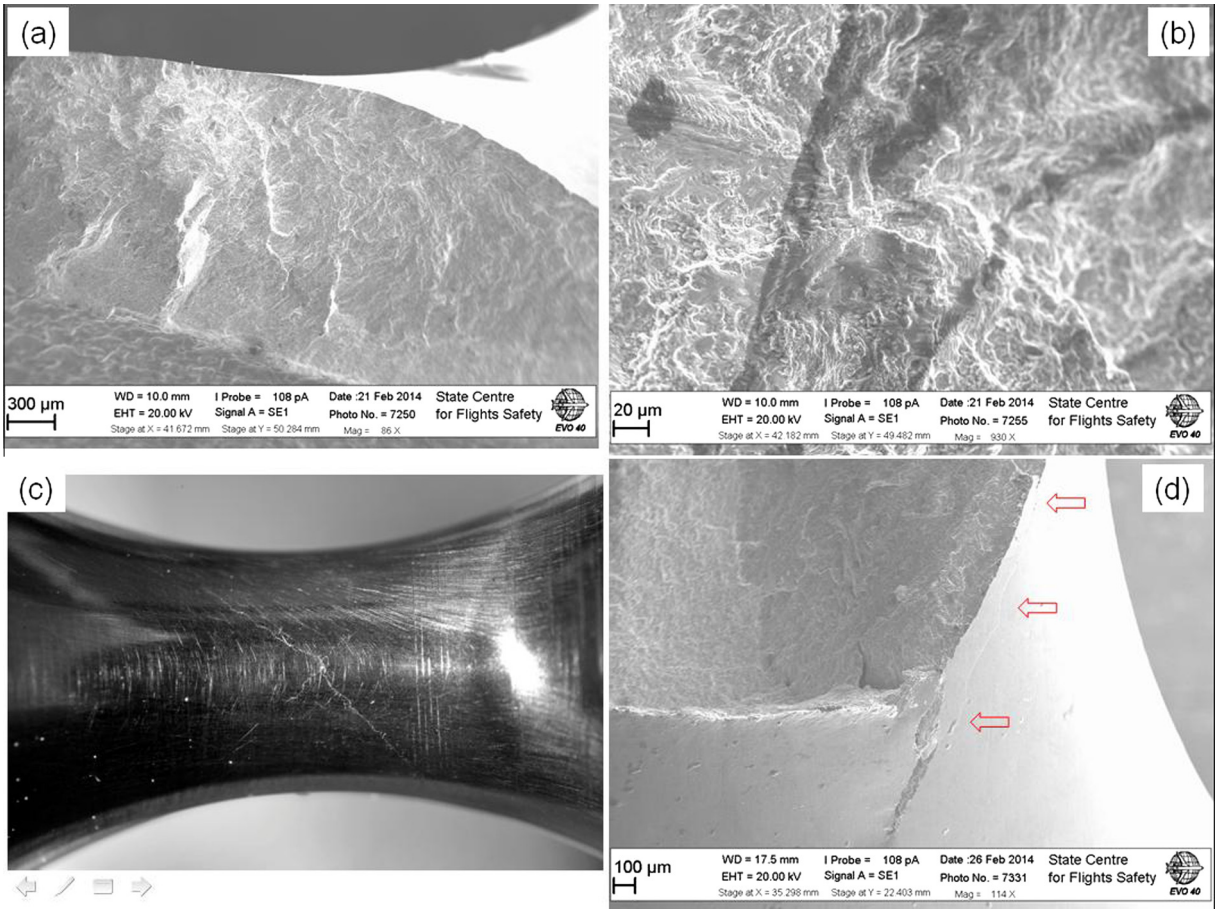

Fig. 9. Torsion crack in forged VT3-1 titanium alloy (a) overview on fracture pattern, (b) crack initiation site, (c) crack path at specimen surface and (d) branching of torsion crack on specimen surface.

macroscopically the main crack is on the maximum normal stress plane. Some secondary cracks that are in competition with the main crack can be observed at the specimen surface, Fig. 9(d). Probably these cracks appear due to the complex microstructure of forged VT3-1.

Like under tensile ($R = -1$) loading the crack path under torsion ($R = -1$) is influenced by the micro-structure. The crack propagates on different levels by forming complex morphology of the fracture pattern. Sometimes torsion crack meets some microstructural elements that were 'walk round' by the crack. Such elements are forcing the crack to propagate on two different planes. It seems that these microstructural elements lead to crack branching that was observed at the specimen surface. But the morphology of the torsion fracture pattern is very perturbed by lips friction that make difficult to distinguish the different stages of crack growth.

4. Conclusion

Based on ultrasonic fatigue results on aeronautical forged VT3-1 titanium alloy in VHCF regime under different loading modes (tensile and torsion) and stress ratios ($R = -1$ and $R = 0.1$) the following conclusions can be proposed:

(1) There are no horizontal asymptotes of the SN-curves for forged VT3-1 under all the tested loading conditions (i.e. no fatigue limits).
(2) The slope of the SN-curve is higher for ultrasonic torsion loading compared to the tensile one.
(3) Both surface and subsurface crack initiation were observed under ultrasonic fatigue testing whatever the load type (tension or torsion). In the case of torsion loading the subsurface crack initiation appears in spite of the maximum shear stress located at the specimen surface.
(4) In the case of subsurface crack initiation under fully-reversed tensile loading ($R = -1$) a multi-modal distribution of fatigue life can be proposed. The following fatigue life controlling mechanisms can be outlined: initiation from (a) agglomeration of rough alpha-platelets (strong defect of micro-structure); (b) border of macro-zones; (c) quasi-brittle facet and (d) smooth facet.
(5) In the presence of tensile mean stress the crack initiation mechanism related to macro-zones becomes a dominant mechanism.
(6) The torsion crack initiation mechanism was not clearly identified for subsurface crack initiation. However a role of structural elements is important in torsion crack propagation. These elements lead to high crack deviation and branching.

References

[1] Schutz W. A history of fatigue. Eng Fract Mech 1996;54(2):263–300. http://dx.doi.org/10.1016/0013-7944(95)00178-6.
[2] Bache MR, Evans WJ. Tension and torsion fatigue testing of a near-alpha titanium alloy. Int J Fatigue 1992;14(5):331–7. http://dx.doi.org/10.1016/0142-1123(92)90485-U.
[3] Shanyavskiy A. Modeling of fatigue failure in metals. In: Synergetic in aeronautic, Monographiya, Ufa; 2007. 498p. ISBN: 978-5-94920-058-2.
[4] Nicolas T. Critical issues in high cycle fatigue. Int J Fatigue 1999;21:S221–31. http://dx.doi.org/10.1016/S0142-1123(99)00074-2.
[5] Shanyavskiy A. Very-High-Cycle-Fatigue of in-service air-engine blades. Science China Physics, Mechanics & Astronomy 2014;57(1):19–29.
[6] Proc. & VHCF-4. August 19–22, 2007. In: John E, Allison J, Wayne Jones, James M. Larsen, Robert O Ritchie, editors. TMS, Ann Arbor, USA; 2007.
[7] Bathias C, Paris PC. Gigacycle fatigue in mechanical practice, Dekker, New-York; 2005. 328p. ISBN 9780824723132.
[8] Bathias C, Drouillac L, Le Francois P. How and why the fatigue S–N curve does not approach a horizontal asymptote. Int J Fatigue 2001;23(Suppl. 1):143–51. http://dx.doi.org/10.1016/S0142-1123(01)00123-2.
[9] Xue HQ, Tao H, Montembault F, Wang QY, Bathias C. Developing of a three-point bending fatigue testing methodology at 20 kHz frequency. Int J Fatigue 2007;29:2085–93. http://dx.doi.org/10.1016/j.ijfatigue.2007.03.018.
[10] Bayraktar E, Xue H, Ayari F, Bathias C. Torsion fatigue behaviour and damage mechanisms in the very high cycle regime. Arch Mater Sci Eng 2010;43(2):77–86.
[11] Bathias C. Piezoelectric fatigue testing machines and devices. Int J Fatigue 2006;28(11):1438–45. http://dx.doi.org/10.1016/j.ijfatigue.2005.09.020.
[12] Russian State Standard GOST-19807-91. Titanium and wrought titanium alloys; 2009.
[13] LeBiavant K, Pommier S, Prioul C. Local texture and fatigue crack initiation in Ti–6Al–4V titanium alloy. FFEMS 2003;25:527–45. http://dx.doi.org/10.1046/j.1460-2695.2002.00480.x.
[14] Nikitin A, Bathias C, Palin-Luc T. A new piezoelectric fatigue testing machine in pure torsion for ultrasonic gigacycle fatigue tests: application to forged and extruded titanium alloys. FFEMS 2015;38(11):1294–304. http://dx.doi.org/10.1111/ffe.12340.
[15] Mayer H, Schuller R, Karr U, Irrasch D, Fitzka M, Hahn M, et al. Cyclic torsion very high cycle fatigue of VDSiCr spring steel at different load ratios. Int J Fatigue 2015;70:322–7 (2015).
[16] Bathias C. There is no infinite fatigue life in metallic materials. FFEMS 1999;22(7):559–65. http://dx.doi.org/10.1046/j.1460-2695.1999.00183.x.
[17] Bathias C. Fatigue limit in metals. Wiley; 2013. p. 128 p. Wiley-ISTE ISBN: 978-1-84821-476-7.
[18] Janecek M, Novy F, Harcuba P, Strasky J, Trsko L, Mhaede M, et al. The very high cycle behaviour of Ti–6Al–4V alloy. Acta Phys Pol, A 2015;128:497–502.
[19] Larsen JM, Jha SK, Szczepanski CJ, Caton MJ, John R, Rosenberger AH, et al. Reducing uncertainty in fatigue life limits of turbine engine alloys. Int J Fatigue 2013;57:103–12.
[20] McEvily AJ, Nakamura T, Oguma H, Yamashita K, Matsunaga H, Endo M. On the mechanism of very high cycle fatigue in Ti–6Al–4V. Scripta Mater 2008;59:1207–9.
[21] Bache MR. A review of dwell sensitive fatigue in titanium alloys: the role of microstructure, texture and operating conditions. Int J Fatigue 2003;25:1079–87.
[22] Oguma H, Nakamura T. The effect of microstructure on very high cycle fatigue properties in Ti–6Al–4V. Scripta Mater 2010;63:32–4.